

1.B Target Experimental System

The target experimental system of the OMEGA Upgrade provides the main facility for performing target experiments, and for acquiring and recording the experimental results. It comprises the following subsystems: the experimental target chamber, the vacuum system, target-positioning systems (for both cryogenic and conventional targets), diagnostic instrumentation, radiation shielding, instrument control and interfacing systems, and the diagnostic control room. In this article, the design considerations for these subsystems are described in detail.

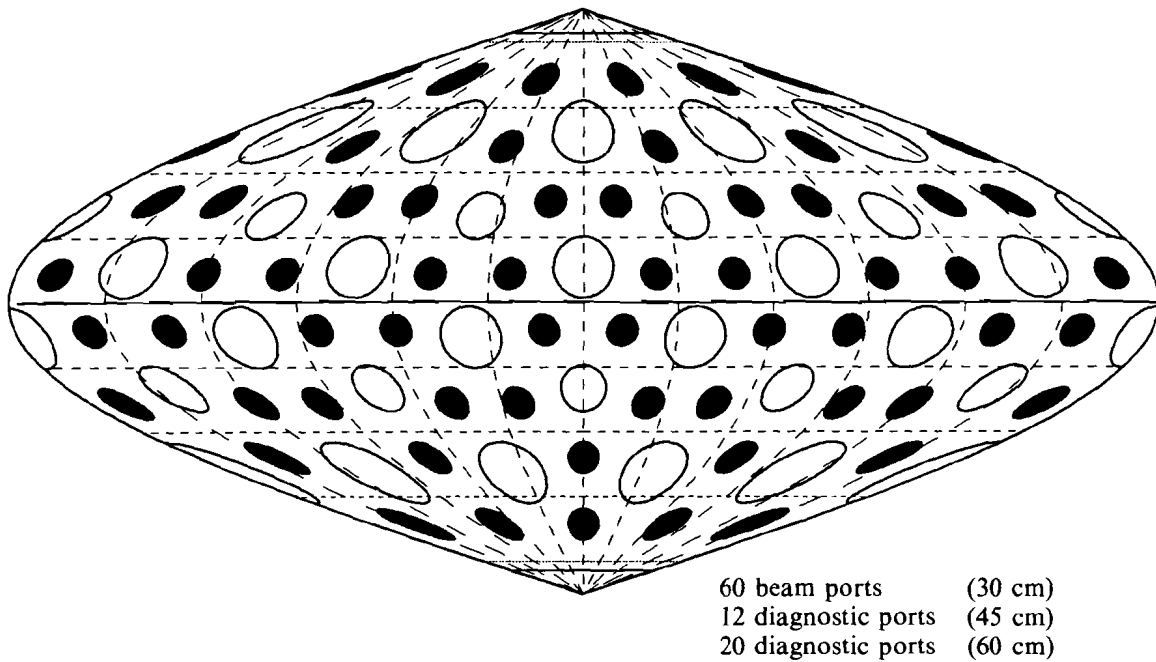
The successful operation of the current OMEGA target experimental facility for the past decade has established a large base of experimental expertise at LLE; this is directly transferable to the OMEGA Upgrade. A new concern is the potential radiological hazards associated with the expected increase in neutron flux. A study has been carried out to address this issue; as a result of this study, additional shielding will be required, and some operating procedures will be revised in order to limit potential radiation exposure to personnel.

Experimental Target Chamber

The design of the experimental target chamber addresses the tasks of target delivery and positioning, stable mounting of the laser-focusing optics, tank pump-down, and containment of radioactive blowoff and target debris. The target chamber will have 60 entrance ports for the laser beams (of 30-cm clear aperture), as well as 20 large-diameter (60 cm) and 12 smaller-diameter (45 cm) ports for diagnostic instrumentation. All of these ports are shown in Fig. 39.9, using a sinusoidal projection. Accurate target positioning in the center of the chamber requires high stiffness and thermomechanical stability of the chamber structure. Precise laser-beam pointing by the chamber-mounted optical assemblies requires better than 10- μ rad pointing stability, which equates to differential chamber deflections of less than 50 μ m under vacuum and instrumentation loading. Additional constraints result from the activation of the target-chamber materials by thermonuclear neutrons and from the possible ablation of the target-chamber surface, thus restricting the choice for the chamber materials.

Several design and fabrication approaches have been compared in terms of cost, performance, nuclear activation, and ease of manufacturing. The acceptable materials from the standpoint of nuclear activation are aluminum 5083, aircraft titanium, possibly 400-series stainless steel, Kevlar®, and other composites. Some of the design trade-offs are given in Table 39.III.

Eastman Kodak has modeled the deflections of the target chamber under vacuum and diagnostic loading using the finite-element code NASTRAN. The modeling of the chamber used a 1/120th section of the chamber that includes three of the chamber ports. Only vacuum



RUN JRP61
TC2662

Fig. 39.9 Sinusoidal projection of beam and diagnostic ports for the OMEGA Upgrade. Beam ports are shown shaded; large and small diagnostic ports are centered on the hexagonal and pentagonal faces, respectively.

(0.1 MPa) loading is applied in this model. The support loads are not included in this model, but since conceivable supports are highly symmetric, they are not expected to significantly alter the total deflections. The results of this analysis for a 10-cm-thick aluminum 6061 alloy chamber are shown in Fig. 39.10. The deflections are within tolerances for pointing and location (10 μ rad).

From the above considerations, Kevlar[®] has been ruled out due to cost and complexity. The leading candidate is presently aluminum 5083, mainly due to its lower fabrication cost. However, if final cost quotes and further research into neutron activation show 400-series stainless steel to be acceptable, the decision will be carefully reviewed with respect to all of the performance trade-offs.

Another problem studied was the ablation of the inner wall of the target chamber, due to material and radiation flux following target shots. Analysis shows that regardless of the wall material, ablation will be insignificant. Figure 39.11 shows the damage threshold of aluminum for soft x rays, for photon energies of up to 100 keV. Here, and in subsequent discussions, the damage threshold is defined to be

Table 39.III Design and fabrication approaches for the OMEGA Upgrade target chamber

Material and Method	Comments
<ul style="list-style-type: none"> • Ti, 1.5–3" thick, welded hemispheres, or welded flat plates (triangle/hex/pent) 	<ul style="list-style-type: none"> – more expensive than aluminum or stainless steel + high stiffness, low activation
<ul style="list-style-type: none"> • Ti, inner/outer skins, internal stiffeners • Al, 3–5" thick, welded hemispheres 	<ul style="list-style-type: none"> – complex welding, expensive + moderate material/machining cost + can be formed and welded + low neutron activation – high-activation weld filler – structural and thermal stability in question
<ul style="list-style-type: none"> • 400 stainless steel ~4" thick, welded hemispheres 	<ul style="list-style-type: none"> + can be formed and welded + good machineability + high stiffness, good stability – more expensive than aluminum – neutron activation (not presently modeled) – may be too heavy for <i>in situ</i> crane – magnetic
<ul style="list-style-type: none"> • Kevlar® winding composite 	<ul style="list-style-type: none"> + low neutron activation – vacuum compatibility and stiffness in question – extremely expensive

E5334

any change in the appearance of the surface that is visible under a high-powered (100X) optical microscope. The damage threshold, as expected, exhibits a minimum near the *K* edge of aluminum, of about 0.7 J/cm^2 . If all the 30 kJ of laser energy were converted into x rays, the flux averaged over the chamber wall would be 0.074 J/cm^2 , lower than the damage threshold for aluminum by a factor of 10.

The same energy loading (0.074 J/cm^2) can be used to estimate the potential damage to the chamber wall due to scattered (unabsorbed) UV radiation. Previous experiments on metal surfaces¹ indicate single-shot optical-damage thresholds of 0.4 J/cm^2 for normally fabricated aluminum surfaces, and 0.9 J/cm^2 for stainless-steel alloy 304. The damage threshold for titanium is not known, but is assumed to be in the same range as aluminum and stainless steel. Diagnostic devices inserted in the OMEGA target chamber experiencing similar irradiation fluences have shown insignificant mass ablation. We believe the dominant effect of the scattered laser light on the chamber wall will be the desorption of gases from the surface.

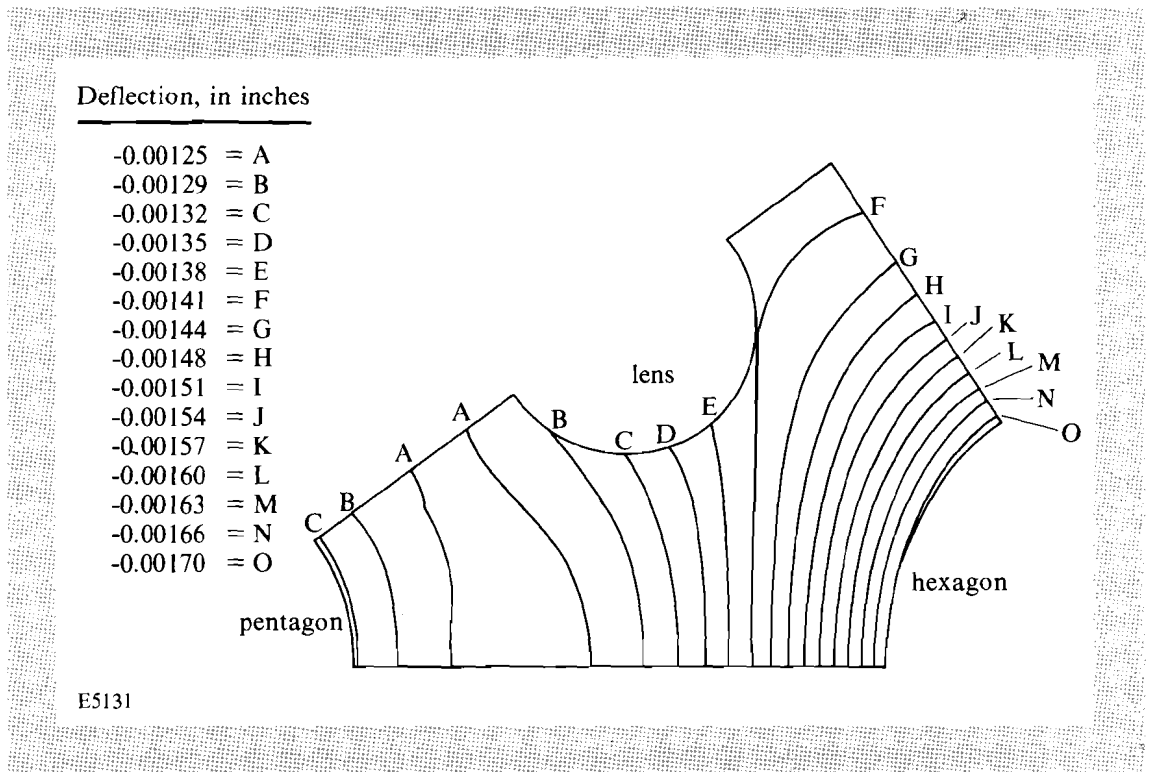


Fig. 39.10
 NASTRAN finite-element analysis of a 1/120th section of the upgrade target chamber. Letters denote lines of equal deflection.

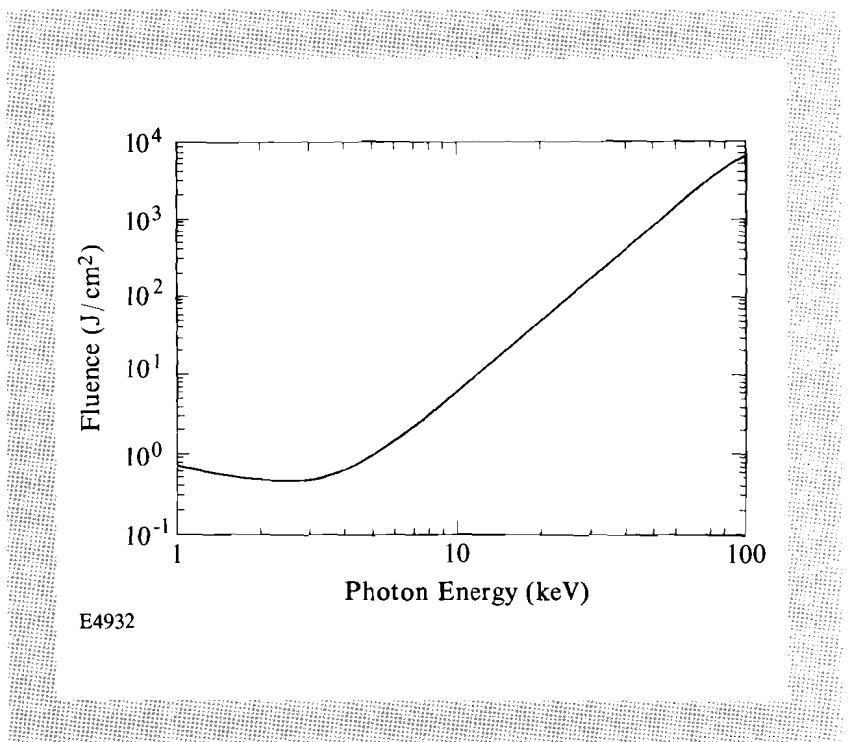


Fig. 39.11
 X-ray damage threshold for aluminum subjected to x rays from laser-target interactions in the range 1–100 keV.

In order to estimate the potential effects of high neutron production we use a “maximum-credible neutron yield” derived by assuming that ignition will be achieved. Using Nuckolls’ definition of ignition,² ignition would imply a gain of ~ 0.3 ; at $\sim 3.5 \times 10^{14}$ neutrons/kJ, the maximum-credible yield is then 3×10^{15} neutrons. The stresses induced in the target chamber due to this flux and the flux of charged reaction products will be negligible compared with those due to the mounting of diagnostic instruments and vacuum loading. The overpressure at the chamber walls resulting from the deposition of 30 kJ of laser energy in the residual gas of the target chamber (which would be 0.01 MPa or 0.1 atm in a worst-case scenario) may be calculated, following Raizer,³ to be 1000 Pa. The resulting shock wave causes negligible additional stress in the chamber walls.

The vacuum system for the upgrade experimental chamber is required to have the capability of evacuating the chamber to an ultimate vacuum of 10^{-4} Pa under no load, and to 10^{-2} Pa with the additional vacuum load presented by diagnostic outgassing and helium refrigerant gas used for cryogenic target preparation. The system must contain and dilute (before effusion to the atmosphere) the expected radioactive blow-off from the diagnostic instruments and the tritium gas from imploded DT-fuel targets. Using a large (60-cm diameter) port located on the bottom of the target chamber, a pumping speed of 20,000 liter/s should be obtained; this will be adequate for handling the highest anticipated loading of helium (2 liter/h of He liquid), which is emitted by the cryogenic target-positioning system. With a 20,000 liter/s pumping speed, the system will cycle from atmospheric pressure to operating vacuum in under 2 hours. The vacuum cycling, monitoring, and interlocking will be controlled by a derivative of the current OMEGA vacuum-control system, WATSON. This system has the ability to interlock, monitor, and automatically cycle critical diagnostics depending on the vacuum state, diagnostic requirements, and utility state. We are currently considering conventional diffusion pumps, with nitrogen or freon-refrigerant cold traps, as well as helium-pumping cryogenic pumps. The modest vacuum requirements that apply to laser-target experiments allow vacuum flanges to be sealed with elastomer O-rings.

In the present OMEGA system, the target chamber is pumped to high vacuum at the beginning of an experimental series, and the system is kept at high vacuum for an extended length of time; targets and diagnostic packages are inserted through vacuum locks. This practice reduces motion of the target chamber due to vacuum loading, provides a more consistent vacuum environment for diagnostics, and minimizes problems associated with the release of radioactive waste into the target-bay area. This mode of operation will be continued for the upgrade target experimental chamber.

Target Positioning and Viewing

The target chamber will include a mechanical positioning system to position targets accurately and with repeatability to within $5 \mu\text{m}$ of the center of the tank. Gas-phase targets will be positioned at the end of a rod of light, low-nuclear-activation material (likely to be a fiber-

composite) by a high-precision 3-axis mechanical positioner located outside the vacuum tank wall.

The cryogenic target-positioning and delivery systems for the OMEGA Upgrade are still under development, but are likely to make use of a combination of techniques employing a retractable cryogenic shroud,⁴ jets of cryogenic helium gas, cold-contact fingers, and various target-heating lasers. The system will allow laser implosions of cryogenically prepared glass microballoons, foam shells and spheres, and various light-metal shells. The positioner will have to conform to stringent requirements of positioning and repeatability (5- μ m centering tolerance), as well as those of operating in a cryogenic environment. Helium refrigerant will need to be delivered to the target positioner through vacuum-insulated cryogenic transfer lines.

In order to optically locate the target in the experimental chamber prior to laser firing, an accurate high-magnification (100X) target-viewing system will be designed. The viewing system should have two orthogonal lines of sight, and be equipped with digital imaging cameras with video frame-grabbers for documentation and analysis. A low-magnification (10X), wide-angle viewing system will also be provided for coarse positioning of the target and diagnostic instruments. The viewing systems will have the ability to locate and align planar and irregularly shaped targets, in addition to spherical targets. In addition to the main viewing systems, which locate targets at the tank center, an auxiliary target positioner/viewer will be provided to locate targets off-center for x-ray backlighting experiments. Augmenting conventional viewing by imaging or shadowgraphy, target quality will be assessed with interferometers along two axes. These interferometers will allow the evaluation of target quality just prior to implosion for both gas-phase and cryogenically prepared transparent targets. Multiple-wavelength illumination systems for these interferometers will be provided, along with digital image readout with frame-grabbers. The current OMEGA system employs three viewing systems similar to that described above. The interferometers currently in use have dual-wavelength capability and are mounted orthogonally to each other; they can view the formation of the cryogenic fuel layer at times up to a few milliseconds prior to the laser firing.

Diagnostic Instrumentation

The target chamber should provide a rigid and stable platform for accurately mounting and positioning all the currently operative diagnostic instruments. The chamber and mounting structure must not preclude introduction of new or novel diagnostics of any reasonable design. The doubly concentric soccer-ball geometry used for the target chamber and for the mirror-mounting structure allows 20 large-diameter (60 cm) diagnostic ports to be located on the hexagonal faces of the target chamber; these ports have clear access out from the target center to a radius of 6-7 m, all the way to the building walls. This free volume available for placing diagnostic instruments will actually exceed that in the present OMEGA system. These large diagnostic ports will be particularly useful for instruments requiring a large solid

angle (such as a high-resolution time-of-flight neutron spectrometer), or they may be fitted with a reducing flange to allow the use of existing OMEGA instruments (see Fig. 39.12). The 12 smaller (45-cm diameter) ports located within the pentagonal faces of the target chamber have clear access out from the target center to a radius of 4.5 m.

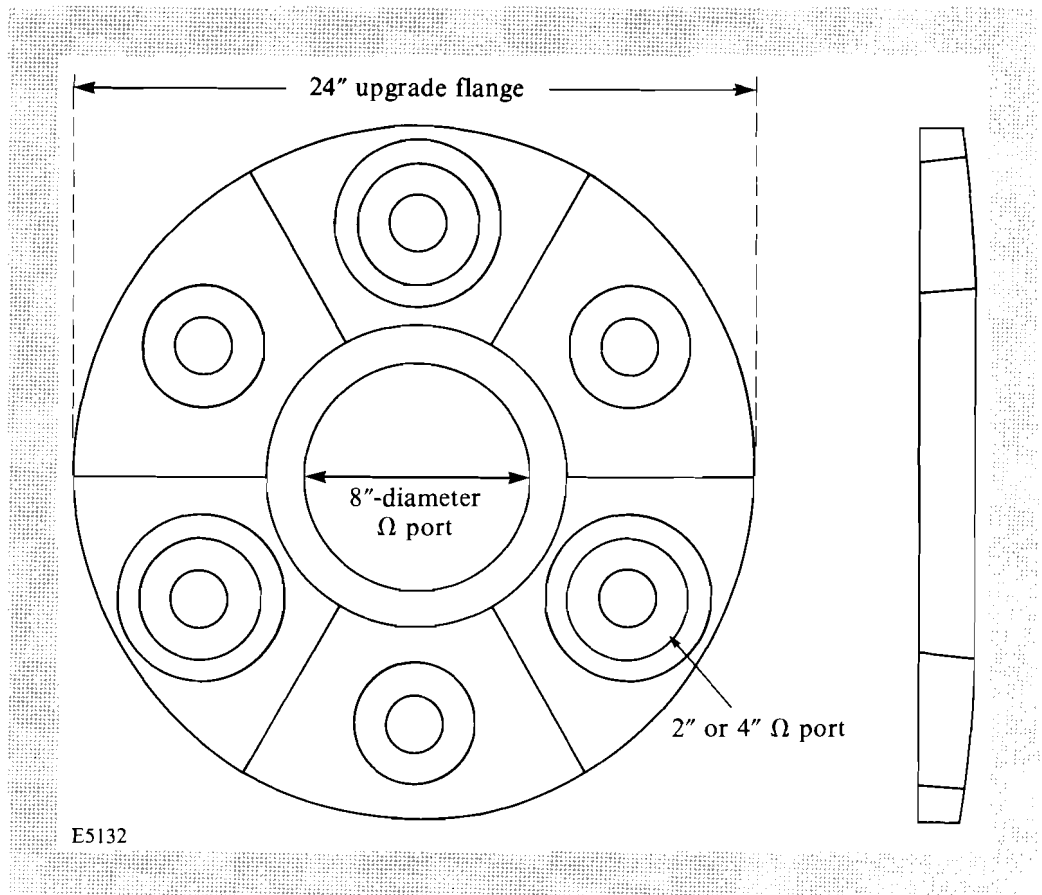


Fig. 39.12

Design of a 24-in. aluminum adapter flange to allow retrofitting of existing OMEGA diagnostic instruments to the upgrade target chamber.

The present complement of nuclear and x-ray diagnostics on OMEGA (see Tables 39.IV and 39.V) will be readily retrofitted to the new chamber, through the use of adapter flanges. Diagnostic devices mounted on the OMEGA Upgrade chamber (of radius 1.8 m) are anticipated to experience x-ray and optical fluences similar to those mounted on the present OMEGA chamber (of radius 0.85 m). The same stringent requirements necessary for the pointing and stability of chamber-mounted final-optic assemblies (0.5-mrad pointing, 50- μ rad vacuum deflection) apply to high-magnification imaging diagnostics.

The expected higher neutron yield from the OMEGA Upgrade system permits the use of new neutron-measuring devices, of greatly increased resolution and accuracy. Table 39.IV lists the major nuclear-diagnostic devices, both those existing on OMEGA and those planned

Table 39.IV Nuclear diagnostics for the OMEGA Upgrade

Measured Parameter Currently on OMEGA	Method	Applicability Range
Fuel areal density	Knock-on	$Y \rho R > 3 \times 10^8 \text{ mg/cm}^2$ $\rho R + \rho \Delta r < 100 \text{ mg/cm}^2$
Shell areal density	Silicon activation	$Y \rho \Delta r > 1.4 \times 10^8 \text{ mg/cm}^2$
Fuel ion temperature	Scintillator-PMT array detector†	$Y > 7 \times 10^8$ $T_i > 1 \text{ keV}$ $Y > 5 \times 10^7$ $T_i > 0.5 \text{ keV}$
Primary yield (in DT)	Cu activation Na activation Ag activation Scintillator-PMT	$Y > 1 \times 10^7$ $Y > 5 \times 10^6$ $Y > 7 \times 10^6$ $Y > 5 \times 10^5$
Secondary yield (in DD)	Scintillator-PMT array detector	$Y > 2 \times 10^5$ $Y > 2 \times 10^5$
Planned for OMEGA Upgrade:		
Neutron imaging	Penumbral image	$Y > 1 \times 10^{12}$
Neutron emission time	Scintillator-PMT	$Y > 5 \times 10^7$
Neutron "burn" width	n-damaged semiconductor neutron streak camera	$Y > 1 \times 10^{12}$ $Y > 1 \times 10^9$

†currently being implemented.

E532I

for the OMEGA Upgrade, and their ranges of applicability. In addition to current diagnostic devices,^{5,6} new single-hit, high-resolution neutron-spectrometer prototypes are currently being tested on the OMEGA system;⁷ these will provide a baseline for performance evaluation of a larger system to be installed on the OMEGA Upgrade. Cable⁸ and Miley⁹ have pointed out the benefits of high-resolution primary, secondary, and tertiary neutron spectroscopy as powerful diagnostics for compressed fuel whose applicability will extend to reactor-scale targets. High-accuracy neutron spectroscopy requires a scattering-free environment for the detector, and a clear flight path through an evacuated tube from the target to the detector. Modeling the flight of neutrons and their interaction with the chamber and its

Table 39.V X-ray diagnostic devices implemented on OMEGA

Spectral Diagnostics	
Diagnostic Device	Range of Measurement (resolution)
3-m grazing incidence spectrograph	12-250 Å
1-m grazing incidence spectrograph	25-300 Å
Imaging crystal spectrograph	0.6-25 Å (20 μm)
Time-resolved (streaked) crystal spectrograph	0.6-25 Å (20 ps)
Total Fluence Diagnostics	
Diagnostic Device	Range of Measurement (resolution)
X-ray calorimeters (2)	0-9 keV
Filtered x-ray diodes (4)	0.1-1 keV (150 ps)
Filtered PIN diodes	1.8-5 keV
Filtered NaI scintillators	5-90 keV
Imaging Diagnostics	
Diagnostic Device	Range of Measurement (resolution)
Kirkpatrick-Baez microscopes (2)	2.5 -12 Å (5 μm)
Pinhole cameras (6)	< 12 Å (15 μm)
Time-resolved multi-frame cameras (2)	3-12 Å (20 μm; 90 ps)
Time-resolved imaging streak camera	3-12 Å (15 μm; 20 ps)
Spectrally resolved pinhole camera	< 12 Å (15 μm; 2.2 Å/mm)

E5322

instrumentation requires Monte-Carlo neutron-transport codes. The distance to the neutron-diagnostic room will be 20-40 m, which will require the construction of a dedicated site outside the target bay (Fig. 39.13). Auxiliary sites along this flight path will be provided for neutron diagnostics at shorter flight paths. With the increase in yields, it should be possible to measure the neutron emission time and neutron "burn" width using techniques developed by groups at Livermore¹⁰⁻¹² and elsewhere.

Characterization of the implosion dynamics of high-convergence OMEGA Upgrade targets and of drive uniformity and symmetry will be carried out using a comprehensive set of x-ray imaging and spectroscopic systems. For the current OMEGA system, time-integrated images with 5-μm resolution, in the wavelength range 2.5-12 Å, are obtained with two Kirkpatrick-Baez microscopes. Six pinhole cameras provide additional coverage below 12 Å, with spatial resolution below 15 μm. One additional multiple-pinhole camera is currently employed in conjunction with an LLNL-developed fast gating system¹³⁻¹⁵ that provides several frames with resolution of 90 ps during an interval of ~1 ns. An x-ray streak camera in combination with an x-ray pinhole provides temporally resolved information on target implosions with one-dimensional spatial resolution.

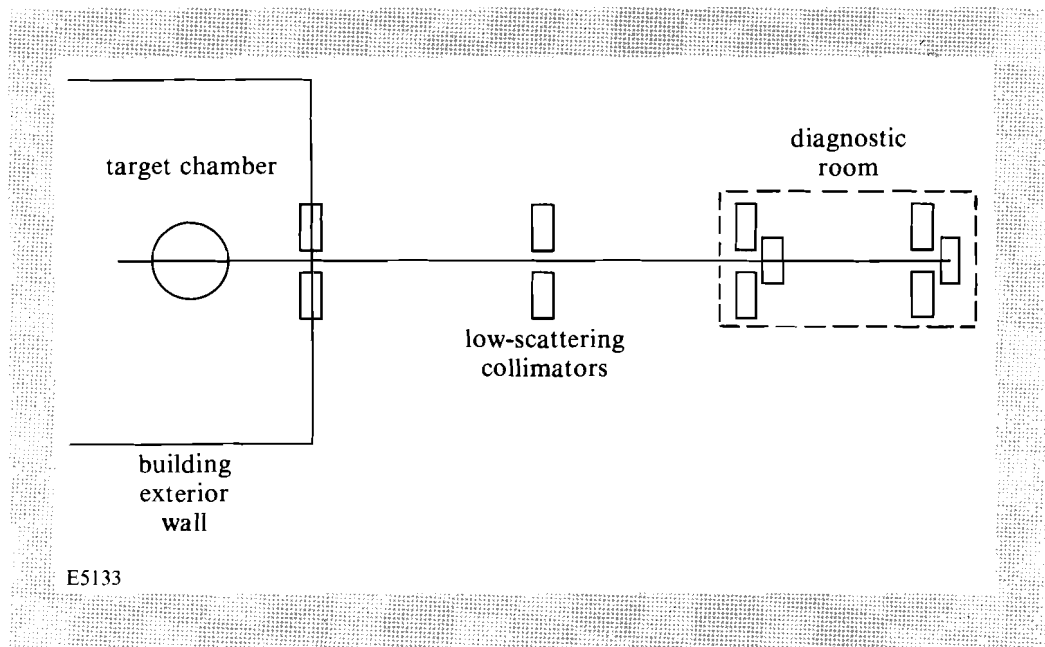


Fig. 39.13

Location of neutron time-of-flight diagnostics outside the present target bay.

Monochromatic x-ray imaging of target implosions is provided by means of a gold x-ray transmission grating in conjunction with an x-ray pinhole camera.

A system for the automatic evaluation of laser pointing on target has recently been developed. It uses a video frame-grabber and microscope to provide an evaluation of the images from several (currently six) views of the target that are provided by x-ray pinhole cameras. Using this system, beams can be reliably positioned to within $15 \mu\text{rad}$ on the target surface in about one hour. The pinhole cameras in use on OMEGA are located approximately 5 cm from the target. In order to avoid ablation problems, the cameras will be moved to 20 cm on the OMEGA Upgrade, where fluences are equal to that on the present OMEGA system. Resolution at this distance (for silicon x rays) is $25 \mu\text{m}$, which is acceptable for targeting: $15 \mu\text{rad}$ accuracy over 1.8 m corresponds to $27 \mu\text{m}$. A similar system will be employed on the upgrade, with more cameras used to allow for accurate placement of all 60 beams.

X-ray spectral-measurement systems, both time-integrated and time-resolved, have been implemented on the current OMEGA system. A novel system incorporating an elliptical crystal and an x-ray streak camera has been developed as a collaborative effort with the NLUF program.¹⁶

Diagnostic instruments that are in close proximity (<20 cm) to the target (pinhole cameras, Kirkpatrick-Baez microscopes, neutron-emission-time detectors, x-ray imaging streak cameras, etc.) will probably experience damage and material ablation under the increased

flux of scattered light, particles, and target debris from the OMEGA Upgrade targets. Moving diagnostics to distances greater than 20 cm, and employing imaging diagnostics with longer image-plane stand-off such as Wolter and Kirkpatrick-Baez microscopes, will assure that they survive.

The OMEGA Upgrade experimental (or diagnostics) control room will be located directly underneath the target chamber, in the area presently housing the diagnostic-control and data-acquisition hardware for the OMEGA system. This location is chosen because of its close proximity to the target chamber. This is important both to save costs and to minimize high-speed signal distortions experienced in long cable lengths. The experimental control room will provide a central data base for the organization of pre-shot and post-shot data, using a local workstation networked to all the other computers of the laboratory. Collection and initial reduction of data from the diagnostic instruments will also be handled by this workstation, in which the CAMAC, General Purpose Interface Bus (GPIB), and RS-232 interfaces will be utilized. Auxiliary terminals and printers will enable prompt inspection and analysis of the data following a target shot, allowing modification of experimental parameters in time for the next target shot. Individual diagnostic instruments will be further controlled locally by smaller computers, to allow for the unloading of various functions from the main workstation controller (these include interlock, vacuum pumps, setup, and protection). Commercial programmable logic controllers are already used for this purpose on some diagnostics on the current OMEGA system.

The prompt nuclear radiation dose projected for the experimental control room may preclude its occupancy during an experiment involving a high-yield DT-fuel target. The networking of the computers in the laboratory will allow the experimental control room to be operated remotely from any location with access to a computer terminal; open access is expected to resume immediately after each shot. The projected silicon dose and dose rate in the present control room is low enough so that upset or damage to any electronic devices will not occur during a shot.

The practices of electromagnetic-interference control that have been successfully adopted for the current OMEGA system will be suitable for the upgrade. The calculated level of electromagnetic interference (EMI) from the upgrade experimental system is no higher than that calculated for the present system, so that additional EMI protection (such as screened rooms, true triaxial or quadraxial cabling, etc.) will not be required.

Nuclear Modeling and Shielding

We have undertaken an extensive joint study with Grumman Aerospace to model the potentially adverse effects of a high level of neutron production on the target chamber and target room, and their surroundings. The modeling employed the one-dimensional discrete neutron-energy-transport code ANISN,¹⁷ in spherical geometry, to study the prompt and activation radioactivity in both silicon

semiconductor devices and biological-tissue samples for several transport scenarios. The modeling used the MONTUK-80 activation-cross-section library, and the MACKLIB-IV response-function library. These data libraries have been developed especially for fusion neutron spectra. The results of the study are given in terms of the prompt dose on silicon and tissue samples, and the nuclear-activation build-up for a typical target-shot schedule.

For the purposes of this study, the relative radiological hazards were determined using health-physics and radiological-dose guidelines from the following sources:

1. Industrial Code Rule 38, Ionizing Radiation Protection (12 NYCRR 38), 1985, State of NY, Department of Labor.
2. Guidelines of the National Council on Radiation Protection and Measurements.
3. Title 10 of the Code of Federal Regulations, part 20 (10CFR20).
4. The "ALARA" (as low as reasonably achievable) recommendation of the International Commission on Radiation Protection.

These sources all quote the following maximum-allowed doses for radiation workers:

1. 3 rem per calendar quarter;
2. total lifetime dose of 5 ($A-18$) rem, where A is the worker's age in years; and for members of the public:
 1. 100 mrem per week;
 2. 2 mrem per hour, whole body.

Based on this guideline, an exposure rate of 2.5 mrem/h is sometimes used to establish a dividing line between restricted-access and free-access areas; however, this level is not listed in any of the regulations.

The modeling assumed maximum-credible neutron yields (based on the achievement of ignition as discussed above) as follows:

for a DT shot:

3×10^{15} neutrons of energy 14.1 MeV and 1×10^{13} neutrons of energy 2.45 MeV;

for a DD shot:

1×10^{13} neutrons of energy 2.45 MeV and 5×10^{10} (secondary) neutrons of energy 14.1 MeV.

Such high yields are not anticipated under routine operating conditions; however, it is important to consider the radiological implication of the upgrade project exceeding its goals.

The experimental chamber, turning-mirror structure, optics, building wall, and associated structures were modeled as spherical shells (Fig. 39.14). These shells were dimensioned to reflect the average radius and composition of the actual structures. Thirteen different path configurations for the neutron transport (see Tables 39.VI and 39.VII)

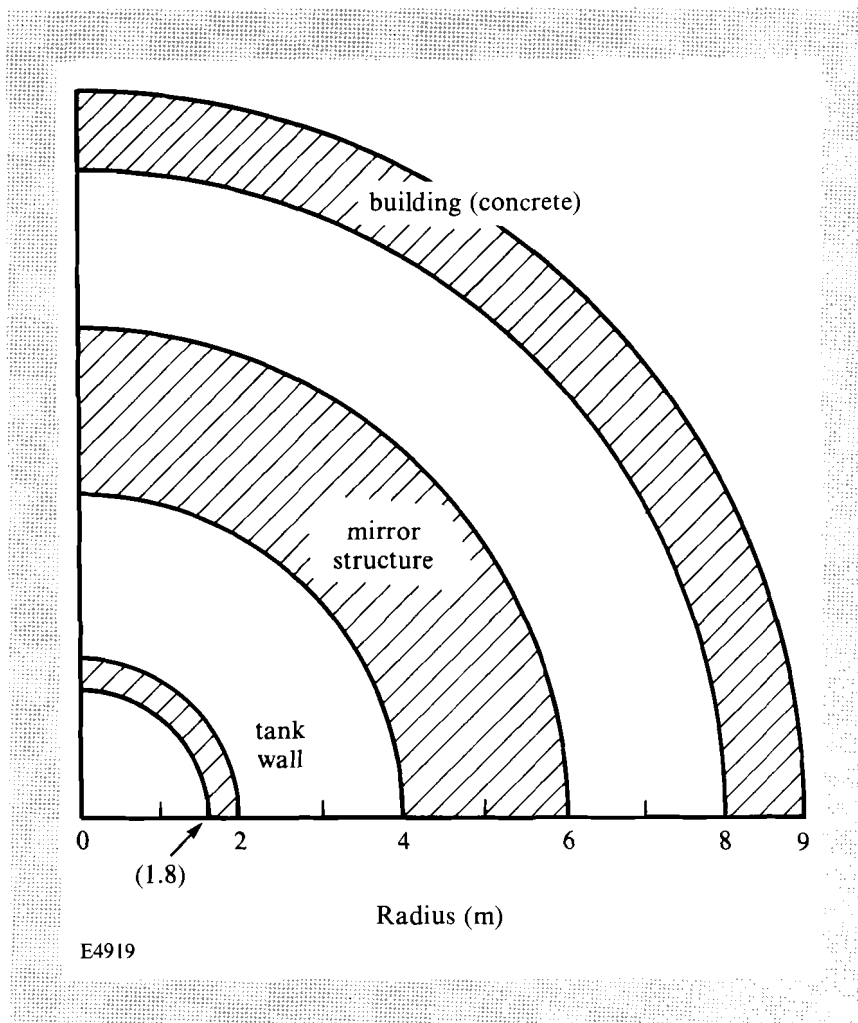


Fig. 39.14
Geometry used for calculating the activation of the target chamber, turning-mirror structure, and building walls.

were modeled. The aluminum components were modeled with aluminum alloy 6061. Since this material has alloying elements that radioactivate more strongly than those in alloy 5083, a worst-case estimate of radioactivity is obtained in the event that some combination of aluminum alloys is used in the final design. The study included the effects on aluminum and steel support structures, and on an assumed experimental chamber constructed of either aluminum or of aircraft titanium of equivalent stiffness. The study assumed that the KDP frequency-conversion crystals would be located near the target, but this option was rejected; the study therefore somewhat overestimates activation levels.

The results of these simulations show that additional shielding will have to be installed in several areas, and some operating procedures will need to be revised in order to limit radiation exposure to personnel. A plan view of the present OMEGA target bay (Fig. 39.15)

Table 39.VI Layer thickness and materials used for ANISN radiation modeling. Layer #1 starts at the target (radius = 0 m).

Geometry	Layer Number			
	1	2	3	4
1	1.8 m vac	10 cm Al	8 m air	
2	1.8 m vac	4.2 m air	5 cm Ti	8 m air
3	6 m air	Optics	Struct. #2	4 m air
4	1.8 m vac	10 cm Al	6.5 m air	Floor
5	1.8 m vac	5 cm Ti	6.5 m air	Floor
6	1.8 m vac	10 cm Al	4.1 m air	Struct. #1
7	1.8 m vac	10 cm Al	4.1 m air	Struct. #1
8	1.8 m vac	5 cm Ti	4.15 m air	Struct. #1
9	1.8 m vac	5 cm Ti	4.15 m air	Struct. #1
10	1.8 m vac	5 cm Ti	4.15 m air	Struct. #2
11	1.8 m vac	5 cm Ti	4.15 m air	Struct. #2
12	1.8 m vac	10 cm Al	4.15 m air	Struct. #2
13	1.8 m vac	10 cm Al	4.15 m air	Struct. #2
	5	6	7	8
1				
2				
3				
4				
5				
6	2.75 m air	Thin wall		
7	2 m air	Thick wall	Thin wall	
8	2.75 m air	Thin wall		
9	Optics	2 m air	Thick wall	Thin wall
10	Optics	2.75 m air	Thin wall	
11	Optics	2 m air	Thick wall	Thin wall
12	Optics	2.75 m air	Thin wall	
13	Optics	2 m air	Thin wall	Thick wall

E5323

shows the lack of adequate shielding along some walls. The use of thick (36–48 in.), movable, keyed, precast-concrete shield blocks in this and other areas that require additional shielding is currently being studied.¹⁸ These blocks are used effectively in high-energy physics laboratories, research reactors, etc. The area directly underneath the target chamber, which presently houses the experimental control area, will have to be operated remotely during a high-yield DT-filled target shot because the prompt tissue dose (30–50 mrem per target shot) would be excessive. The thin-wall building-leakage dose rate (position C on Fig. 39.15) is less than 1 mrem per DT shot with the additional shield walls in place.

Table 39.VII Material terms glossary (used in Table 39.VI)

Al	=	6061 aluminum alloy
Ti	=	aircraft titanium
Optics	=	4 cm fused silica (vacuum window), 7.5 cm fused silica (lens and distributed phase plate), 5 cm KDP (frequency-conversion cell)
Struct. #1	=	5 cm 1040 (mild) steel
Struct. #2	=	7.5 cm Al, 2.5 cm 1040 steel
Thin wall	=	20 cm cinder block, 10 cm brick facia
Thick wall	=	76.2 cm reinforced concrete (reinforcement bars, 1020 mild steel, 1.3-cm diam on 20-cm center-center spacing)
Floor	=	same as thick wall
Air	=	air at atmospheric pressure
Vac	=	vacuum (1×10^{-2} Pa)

E5324

Modeling has further been performed to estimate the effects of the high neutron and n -gamma prompt dose rate on electronics and optoelectronics in the vicinity of the experimental chamber. It is likely that within a 20-cm radius of the imploded target, upset and/or permanent damage to electronics will occur. The silicon dose and dose rate for electronics at the wall of the target bay is acceptable for all types of microelectronics, with the exception of power transistors, silicon-controlled rectifiers, and other silicon devices of large junction area. Electronics employing such devices will be transferred to the area beneath the target-bay floor.

Neutron activation of the target chamber, support structure, and surroundings determines the maximum-acceptable number of shots in a given time period, and the minimum time following a target shot, before personnel are allowed reentry into the target bay. Data for a typical activation analysis is presented in Fig. 39.16, for the following experimental scenario:

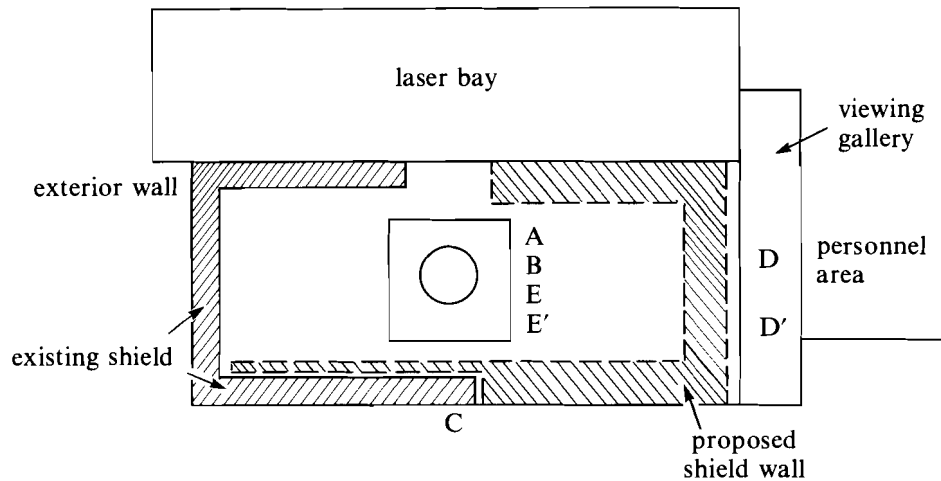
One DT-fuel target and four D₂-fuel targets per day (2-h shot cycle).

Three days of experiments per week (Monday, Wednesday, and Friday).

Two weeks of experiments, followed by one week of no target shots.

A one-month shut-down period at the end of a 48-week period of experiments.

The modeling follows this cycle for a full year, evaluating the buildup and decay of nuclear products in the target chamber, the support structure, and the exterior wall of the building. Figure 39.16 shows the cycle of activation and decay following each shot for a section of



Doses for Maximum-Credible Yield (3×10^{15} neutrons)

- A - 0.08 rem (beneath floor)
- B - 46 rem (above floor)
- C - 0.0005 rem
- D - 4.3 rem
- D' - 0.0005 rem (with proposed shield wall)
- E - 9.7 rem (ceiling)
- E' - 0.002 rem (at 2000')

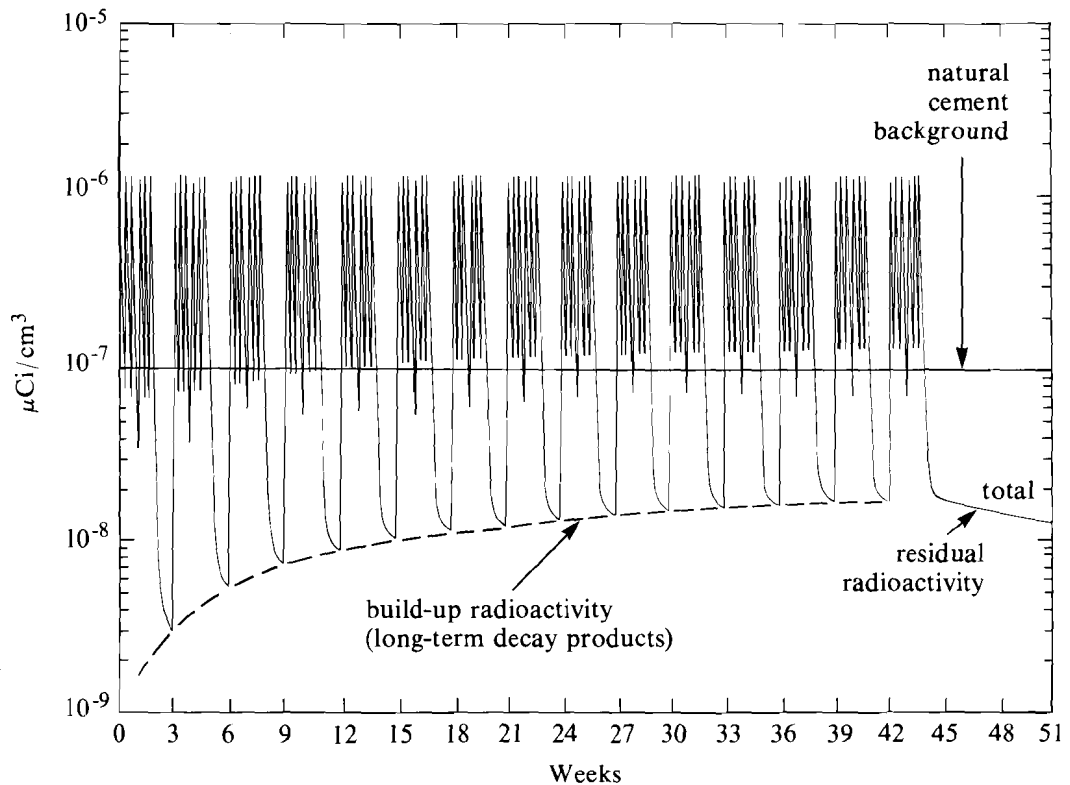
E5137

Fig. 39.15

Personnel doses for a DT target shot with a maximum-credible yield of 3×10^{15} neutrons. Location A is in the present diagnostic control room; location E' is for an aircraft at an altitude of 2000 ft above the target chamber. The shaded areas indicate the location of proposed movable shielding around walls of the target bay.

the thick reinforced cement shield wall modeled on neutron flight paths 7, 11 and 13. For comparison, the normal level of radioactivity for natural cement in this area is about $1 \times 10^{-7} \mu\text{C}/\text{cm}^3$. The shield wall represents one of the worst areas for radioactivity because of the long half-life decay products and large mass. Analysis of this data indicates that a "cool down" period of 0.5–1 h between implosion and personnel reentry into the target bay is required.

Nuclear activation of the air in the target bay has also been considered in this study. Following a high-yield DT-filled target shot, the air in the vicinity of the target chamber will be activated to about $15 \mu\text{C}/\text{m}^3$ (due to the activation of the nitrogen isotope N^{13} , which decays with a half-life of 9.95 min). Activation of the air to this level will require an extension of the cool-down cycle duration.



E5141

Fig. 39.16

Activation analysis of the shield-wall material for a projected year of experiments, showing the buildup and decay of radioactive products at the exterior wall for the assumed daily, weekly, and yearly schedule. The spikes are due to short half-life radionuclides, primarily from the reaction $\text{Na}^{23}(n,\gamma)\text{Na}^{24}$. The build-up residual radioactivation is due to the longer half-life reactions $\text{Ca}^{40}(n,\alpha)\text{Ar}^{37}$, $\text{K}^{39}(n,T)\text{Ar}^{37}$ and $\text{Ca}^{44}(n,\gamma)\text{Ca}^{45}$.

Because of the low-level radiation hazard that may exist following an implosion involving thermonuclear reactions, radiation-monitoring equipment will be installed in the target bay, air plenums, and in adjacent areas, to monitor the prompt and activation doses. The monitoring equipment will include tritium (beta-decay) detectors placed near the target bay to check for radioactivity of diagnostic instruments outside the experimental chamber; prompt neutron and gamma-ray total-dose detectors (calorimeters) placed in the target bay and nearby areas; and filtration-type air-sampling equipment for monitoring air activation in the plenums leading to and from the target bay. Similar detectors will be located in the areas of the laser bay that are unshielded and in proximity to the target chamber. These detectors will be connected to computer-controlled interlocks, in order to eliminate the possibility of inadvertent entry of personnel during cool-down periods. These precautions will allow operation at the maximum shot rate consistent with personnel safety.

ACKNOWLEDGMENT

This work was supported by the U.S. Department of Energy Office of Inertial Fusion under agreement No. DE-FC03-85DP40200 and by the Laser Fusion Feasibility Project at the Laboratory for Laser Energetics, which has the following sponsors: Empire State Electric Energy Research Corporation, New York State Energy Research and Development Authority, Ontario Hydro, and the University of Rochester. Such support does not imply endorsement of the content by any of the above parties.

REFERENCES

1. J. F. Figueira and S. J. Thomas, *IEEE J. Quantum Electron.* **QE-18**, 1381 (1982).
2. J. H. Nuckolls, Lawrence Livermore National Laboratory Report UCRL-84932 (1980).
3. Y. P. Raizer, *Sov. Phys. JETP* **21**, 1009 (1965).
4. LLE Review **33**, 11 (1987).
5. LLE Review **27**, 103 (1986).
6. LLE Review **36**, 150 (1988).
7. R. Kremens and M. Russotto, presented at the 31st Annual APS meeting of the Plasma Physics Division, Anaheim, CA, 13-17 November 1989.
8. M. D. Cable, *J. Appl. Phys.* **60**, 3068 (1988).
9. D. R. Welch, H. Kislev, and G. H. Miley, *Rev. Sci. Instrum.* **59**, 610 (1988).
10. D. R. Kania *et al.*, *IEEE Trans. Nucl. Sci.* **35**, 387 (1988).
11. C. L. Wang *et al.*, *Rev. Sci. Instrum.* **57**, 1749 (1986).
12. G. L. Tietbohl, R. A. Lerche, and S. M. Lane, *Bull. Am. Phys. Soc.* **33**, 1868 (1988).
13. J. D. Kilkenny *et al.*, *Rev. Sci. Instrum.* **59**, 1793 (1988).
14. D. K. Bradley, J. Delettrez, P. A. Jaanimagi, F. J. Marshall, C. P. Verdon, J. D. Kilkenny, and P. Bell, *High Speed Photography, Videography, and Photonics VI* (SPIE, Bellingham, WA, 1988), Vol. 981, p. 176.
15. P. E. Bell, J. D. Kilkenny, G. Power, R. Bonner, and D. K. Bradley, *Ultra High Speed, High Speed Photography and Videography and Photonics VII* (SPIE, Bellingham, WA, 1989), to be published.
16. B. L. Henke and P. A. Jaanimagi, *Rev. Sci. Instrum.* **56**, 1537 (1985).
17. ANISN, Oak Ridge National Laboratory.
18. Radiological Safety in the Design and Operation of Particle Accelerators, NBS Handbook 107, revised 1978, U.S. Department of Commerce.